Composites Science and Technology 173 (2019) 47–52

Contents lists available at ScienceDirect

Composites Science and Technology

journal homepage: www.elsevier.com/locate/compscitech

Lightweight, strong, and super-thermal insulating polyimide composite aerogels under high temperature

Wei Fan, Xiang Zhang, Yi Zhang, Youfang Zhang, Tianxi Liu*

State Key Laboratory for Modification of Chemical Fibers and Polymer Materials, College of Materials Science and Engineering, Innovation Center for Textile Science and Technology, Donghua University, 2999 North Renmin Road, Shanghai 201620, PR China

ARTICLE INFO

Keywords:
A: Nano composites
A: Polymer-matrix composites (PMCs)
B: Thermal properties
B: Mechanical properties
Aerogels

ABSTRACT

High-performance thermally insulating materials is highly desirable for many applications in which heat transfer should be strictly restricted. Traditional organic or inorganic insulation materials are limited by either poor thermal stability or mechanical brittleness. Here, SiO_2 nanoparticles crosslinked polyimide aerogels synthesized by one-pot freeze-drying are presented, which show excellent mechanical properties and super-insulating behavior in a wide temperature range. The highly porous structure of the aerogel and nanosized components benefit the significant reduction of thermal conductivity through inhibiting gas conduction and imparting interfacial thermal resistance, respectively. The PI/SiO_2 composite aerogel with a density of 0.07 mg cm^{-3} can achieve a low thermal conductivity of 21.8 mW m^{-1} K^{-1}, which is lower than the most common super-insulating criterion (25 mW m^{-1} K^{-1}). More importantly, the PI/SiO_2 aerogel exhibits good thermal insulation performance at elevated temperatures, with a thermal conductivity still lower than 35 mW m^{-1} K^{-1} even at 300 °C. Therefore, the mechanically strong and super-insulating PI/SiO_2 composite aerogels are promising candidates for practical thermal insulation applications.

1. Introduction

Decreasing heat transfer via advanced thermal insulators is one efficient approach to improve the energy efficiency and reduce the world's total energy consumption, which contributes to a lower carbon footprint [1–3]. Advanced thermal insulators are also urgently needed for many optical, electrical and space applications in which heat transfer should be strictly restricted [4–8]. Therefore, developing materials with a superior insulation performance is highly desirable, which possess thermal conductivity (λ) values below those of commercially available insulation materials, such as polyurethane (PU) foam, expanded polystyrene, mineral wool and fiberglass (λ = 30–50 mW m^{-1} K^{-1}).

Aerogels are believed to be ideal candidates for thermal insulation due to their high porosity (80.0–99.9%) and low apparent density (0.003–0.15 g cm^{-3}) [9–11]. Currently, typical silica aerogels are widely studied and exhibit good thermal insulation properties with a low λ of 17–21 mW m^{-1} K^{-1} under ambient conditions, but their potential applications are severely restricted by the poor mechanical properties [12–17]. The emerging organic aerogels show better mechanical properties, but have a slightly higher thermal conductivity of 20–40 mW m^{-1} K^{-1} as compared to silica aerogels [18]. Moreover, typical organic aerogels, such as PU aerogels [19,20], cellulose aerogels [21–23], poly(vinyl alcohol) aerogels [24,25], exhibit poor thermal insulation performance under elevated temperatures, which tend to collapse at temperature above 200 °C. Although the thermal stability of organic aerogels can be improved by incorporating inorganic fillers, such as silicate and clays, current organic aerogels cannot be stable over 300 °C [26–30]. More recently, some works have presented super-insulating materials (λ as low as ~21 mW m^{-1} K^{-1}) such as bioinspired polymeric woods [31] and anisotropic nanowood [1], but their insulation behavior at elevated temperature has not been studied. Therefore, aerogel materials with both excellent thermal insulation behavior under a wide temperature range and good mechanical properties are urgently required, which is highly desirable in many applications where much higher using temperatures are needed.

Polyimide (PI) aerogels exhibiting excellent mechanical properties (Young's modulus over 100 MPa), low thermal conductivity (30–60 mW m^{-1} K^{-1}) and high-temperature stability (up to 600 °C) have drawn much attention recently [32–37]. These properties make robust PI aerogels promising candidate for thermal insulation applications, especially under high-temperature circumstance. However, further decreasing the thermal conductivity of PI aerogels has reached a plateau since it would lead to compromises in mechanical properties

* Corresponding author.
E-mail addresses: txliu@dhu.edu.cn, txliu@fudan.edu.cn (T. Liu).

https://doi.org/10.1016/j.compscitech.2019.01.025
Received 26 September 2018; Received in revised form 14 January 2019; Accepted 23 January 2019
Available online 26 January 2019

and fabricating complexity. Typically, PI aerogels have been synthesized from dianhydrides and diamines, followed by chemical imidization and supercritical drying [38]. Normally polyimide aerogels prepared from supercritical carbon dioxide drying exhibit a nanofibrous structure while their porous structure cannot be well controlled. Different from supercritical drying, freeze-drying method is a promising alternative since it is cost effective and environmentally friendly [39,40]. However, the formation of PI aerogels usually suffers from large shrinkage, which contributes to the loss of porosity and strength. Since the thermal insulation performance of aerogels is highly related to their porous structure, alternative approaches to fabricate PI aerogels with less shrinkage and well-organized porous structure via freeze-drying is still a challenge.

Previous work has shown that inorganic nanoparticles, such as clay nanoplatelets and graphene sheets, can perform as crosslinking agents for polymer gels, which helps to improve structural stability and mechanical properties of the gel [41,42]. The inorganic nanoparticles behaving like crosslinkers could inhibit shrinkage and maintain the high porosity of aerogels, which favors the improvement of thermal insulation. More importantly, it has been reported that the use of nanosized components can effectively reduce heat conduction of pore walls through imparting interfacial thermal resistance [2]. More recently, hollow mesoporous silica nanoparticles crosslinked PI aerogels have been reported with improved mechanical properties and low thermal conductivity via supercritical carbon dioxide drying [43]. Therefore, incorporating inorganic nanoparticles into PI aerogels could further reduce their thermal conductivity, without sacrificing the mechanical properties and thermal stability. However, the effect of crosslinkers on the porous structure as well as corresponding thermal properties have not been studied yet.

Herein, inorganic SiO_2 nanoparticles crosslinked polyimide aerogels have been synthesized by one-pot freeze-drying followed by thermal imidization. SiO_2 nanoparticles as crosslinkers could effectively control the porous structure and subsequently optimize thermal properties of aerogels. The crosslinking points formed from interactions between amino functionalized SiO_2 nanoparticles and PI chains favor the formability of PI/SiO_2 composite aerogels, which exhibit a little shrinkage ($< 20\%$) and a well-organized honeycomb-like porous structure. The thermal conductivity of PI/SiO_2 composite aerogel can be optimized by tuning the porous structure via crosslinking points, achieving a low thermal conductivity of 21.8 $mW\,m^{-1}\,K^{-1}$. More importantly, the thermal conductivity of PI/SiO_2 aerogel only shows a slight increase as the temperature goes up, with a thermal conductivity still lower than 35 $mW\,m^{-1}\,K^{-1}$ at 300 °C. The super-insulation properties of PI/SiO_2 composite aerogel at room and high temperatures make them promising candidates for thermal insulation applications.

2. Experimental section

2.1. Fabrication of PI/SiO_2 composite aerogels

Silica nanoparticles were first functionalized by 3-aminopropyltriethoxysilane (3-APTS) to obtain amino functionalized silica nanoparticles (NH_2-SiO_2) (see details in supporting information). PI/SiO_2 composite aerogels were prepared according to our previous work [39,40]. Briefly, water-soluble poly(amic acid) (PAA) oligomer (synthesis procedure illustrated Fig. S1), was mixed with functionalized silica nanoparticles to obtain a homogenous PAA/SiO_2 sol. PI/SiO_2 composite aerogels was obtained by subsequent freeze-drying and thermal imidization process. PI composite aerogels with 0, 10, 20, and 30 wt% loading amount of NH_2-SiO_2 nanoparticles were fabricated, and denoted as PI, PI/SiO_2-1, PI/SiO_2-2, and PI/SiO_2-3, respectively.

3. Results and discussions

Different from the usually used supercritical drying method, a green freeze-drying method is employed to prepare PI aerogels in this work. Water-soluble poly(amic acid) oligomer is dissolved in deionized water and kept for gelation at room temperature. The PAA hydrogel is subsequently freeze-dried and thermally imidized to obtain PI aerogel. The influence of the concentration of PAA in the hydrogel on the morphology of as-obtained PI aerogel is first investigated. SEM images of PI aerogels prepared from PAA concentration of 10, 7, 5, 4 wt% are shown in Fig. S2 and the corresponding pore size distribution are shown in Fig. S3. It can be observed that honeycomb-like porous structures are formed for all the aerogels. However, PAA with high concentrations exhibits high viscosity, which lead to non-uniform ice growth rate in the freeze-drying process, resulting in the inhomogeneous porous structure and thick pore walls of corresponding PI aerogel (Figs. S2a and 2b). PI aerogels prepared from PAA hydrogel with 5 wt% concentration show a much more uniform porous structure (Fig. S2c) with smaller pore size mainly centered in 15 μm (Fig. S3c) and less shrinkage (Fig. S4). Further decreasing the concentration of PAA results in the increase of pore size (30 μm) of PI aerogel since diluted solution favors formation of larger ice crystals (Figs. S2d and 3d). Therefore, unless specifically stated, PI aerogels prepared from PAA hydrogel with 5 wt% concentration, exhibiting uniform porous structure and less shrinkage, are used in the following text.

Before fabricating PI/SiO_2 composite aerogels, SiO_2 nanoparticles were first functionalized by 3-APTS to enhance the interaction between SiO_2 nanoparticles and polymer chains. SEM image shows SiO_2 nanoparticles are 10–20 nm in size (Fig. S5a) and FTIR spectra prove successful functionalization of SiO_2 nanoparticles (Fig. S5b). Compared with pure SiO_2, additional peaks located at 2980-2850 cm^{-1} and 1190 cm^{-1} of functionalized SiO_2 are associated to C-H and C-N stretching modes, indicating that amino groups (-NH_2) are grafted onto SiO_2 nanoparticles. The NH_2-SiO_2 nanoparticles were subsequently mixed with PAA precursor to fabricate PI/SiO_2 composite aerogels as illustrated in Fig. 1.

The morphology of PI/SiO_2 composite aerogels with different loading of SiO_2 is shown in Fig. 2a–d. All the aerogels exhibit honeycomb-like porous structures with the pore size varied by adding different amount of SiO_2. Neat PI aerogel shows a large pore size in the range of 10–20 μm with a broad distribution (Fig. 2a). With SiO_2 nanoparticles, the composite aerogels exhibit smaller pore sizes and more uniform distributions, with PI/SiO_2-2 composite aerogel exhibiting the smallest pore size of ~9 μm among those samples (Fig. 2b and c). TEM images of PI/SiO_2-2 aerogels (inset in Fig. 2c and Fig. S6) verify SiO_2 loaded in PI and indicate the uniform dispersion of SiO_2 nanoparticles in PI matrix. However, further increasing the amount of SiO_2 nanoparticles leads to the slight increase of pore size (~13 μm) as for PI/SiO_2-3, which is probably due to the aggregation of SiO_2 nanoparticles in PI matrix as indicated by the inset in Fig. 2d. The smaller pore size of PI/SiO_2-2 composite aerogel is attributed to the strong interaction between polymer chains and functional groups on SiO_2 nanoparticles as well as steric effect of inorganic SiO_2 as schematically illustrated in Fig. 2e. Theoretically speaking, the porous structure of aerogels is highly dependent on structural planarity and intermolecular interaction formed during the gelation process [44]. In the PAA/SiO_2 hydrogel, physical or chemical interactions between PAA and NH_2-SiO_2 nanoparticles through hydrogen bond and amide bond can form crosslinking points, which could maintain the 3D interconnected structure during the freeze-drying process, thus forming a porous structure. More functional groups on SiO_2 nanoparticles lead to increased crosslinking points formed in the hydrogel, thus forming a smaller pore size in the final aerogel. The chemical interaction between PAA chain and NH_2-SiO_2 nanoparticles can be inferred from the XPS characterization (Fig. S7). As compared with PAA, the intensity of C-N bond increased while the intensity of O-C=O bond decreased for PAA/SiO_2 composite, indicating more amide bond formed between PAA chains and NH_2-SiO_2 nanoparticles.

The structural formability and mechanical properties of PI/SiO_2

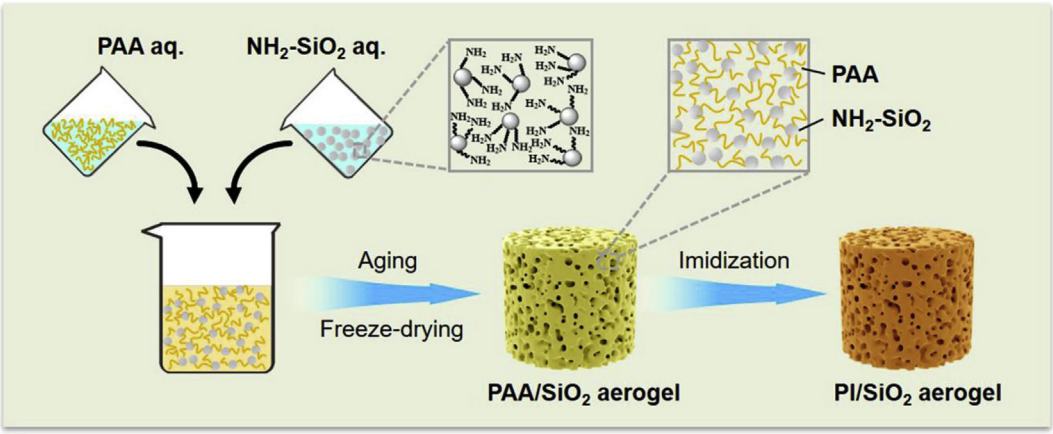

Fig. 1. Schematic illustration for preparation of PI/SiO_2 composite aerogels.

composite aerogels are investigated in Fig. 3 and Table S1. The aerogels show very low density of ~0.07 g cm^{-3} and good structural formability, which can be shaped into letters of DHU (Fig. 3a). The lightweight aerogel can withstand 7000 times of its own weight, indicating excellent anti-compressibility (Fig. 3b). As shown in Fig. 3c, the shrinkage of PI/SiO_2 composite aerogels is less than 20%, much smaller than that (32%) of neat PI aerogel. Silica nanoparticles in polyimide matrix are treated as the crosslinker, which play dual roles for reducing the shrinkage of the polyimide gels. First, crosslinking points formed between PAA and functionalized SiO_2 would maintain the 3D interconnected structure during drying. Second, SiO_2 nanoparticles help to inhibit the stacking between polymer chains (steric effect), which inhibits the shrinkage and maintain a uniform porous structure. Consequently, PI/SiO_2-2 aerogels exhibit a high porosity up to 96%. The strain-stress curves shown in Fig. 3d indicate that the PI/SiO_2 aerogels can be compressed by 80% or more without catastrophic collapse. The compression modulus calculated from the linear part of strain-stress curve of PI/SiO_2-2 composite aerogel is about 30.4 ± 2.9 MPa, which is much higher than that (0.7–12 MPa) of previously reported polyimide-silica hybrid aerogels with similar density [45,46]. The specific compression modulus represents the ratio of compression modulus to apparent density, which can better indicate the mechanical properties for ultralight materials. The specific modulus of PI/SiO_2-2 aerogel is 384 kN m kg^{-1}, which is substantially higher than most aerogel materials as listed in Fig. 3e, normally exhibiting specific modulus less than 100 kN m kg^{-1}.

Aerogels are one of the most excellent thermal insulation materials, with significantly low thermal conductivity due to their high porosity. As shown in Fig. 4a, pure PI aerogel with a density of ~0.1 g cm^{-3} shows a thermal conductivity (λ) of 52.8 mW m^{-1} K^{-1}, which is comparable to the commercial insulation materials like expanded polystyrene (35–55 mW $m^{-1}K^{-1}$) and glass wool (38–50 mW m^{-1} K^{-1}).

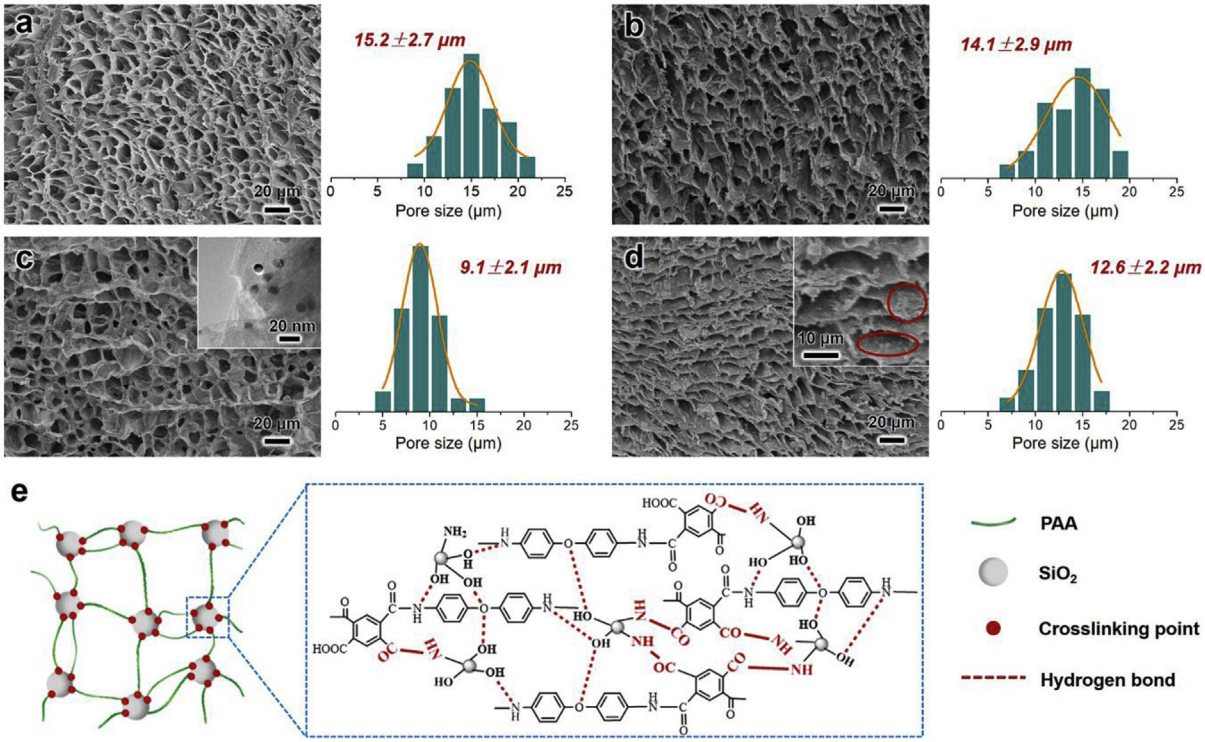

Fig. 2. Morphology and structural characterization of PI/SiO_2 aerogels. (a–d) SEM images and corresponding pore size distribution of PI/SiO_2 composite aerogels with different loading of SiO_2. (a) PI, (b) PI/SiO_2-1, (c) PI/SiO_2-2, and (d) PI/SiO_2-3. Inset in Fig. 2c shows the corresponding TEM image of PI/SiO_2-2. (e) Schematic illustration for porous structure of aerogel and interaction between PI chains and functionalized SiO_2 nanoparticles.

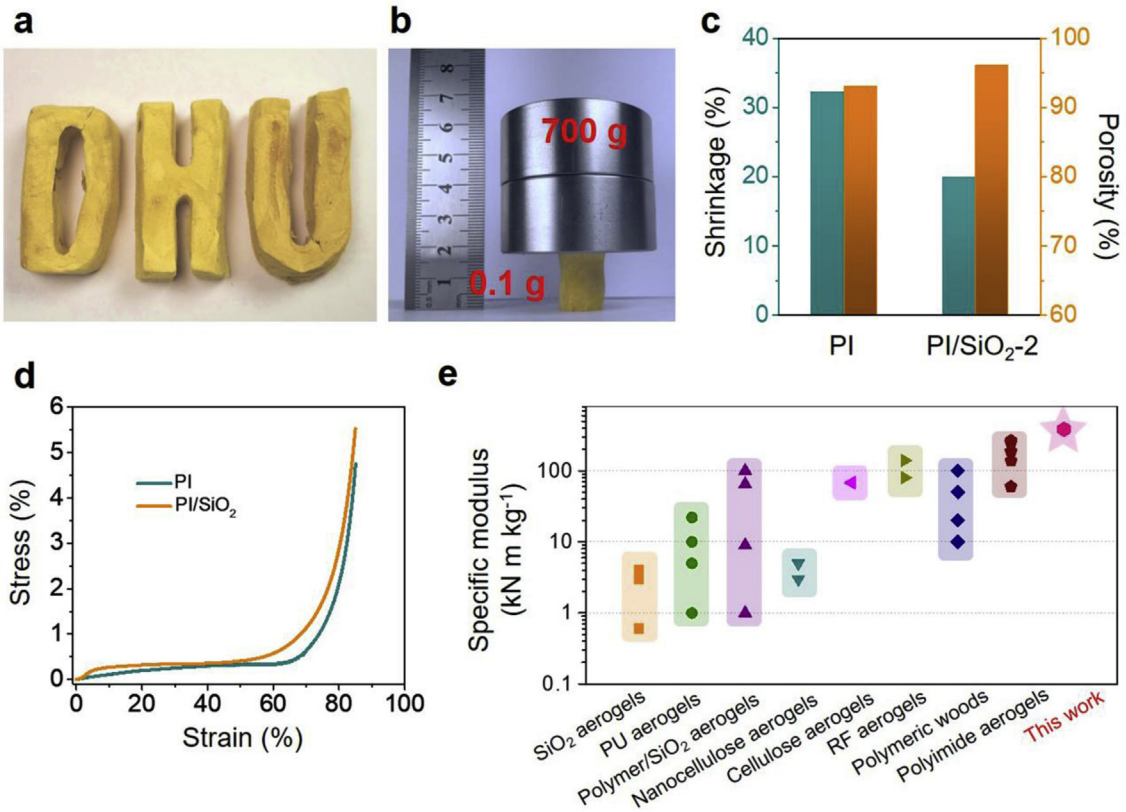

Fig. 3. Dimensional stability and mechanical properties of PI/SiO_2 aerogels. (a) Digital photo of PI/SiO_2 aerogels that can be shaped into letters of DHU. (b) Digital photo showing the PI/SiO_2 aerogel compressed by an ion block. (c) Shrinkage and porosity of PI and PI/SiO_2 aerogels. (d) Strain-stress curves of PI and PI/SiO_2 aerogels. (e) Comparison of specific modulus of our PI/SiO_2 aerogel to common aerogel-like materials, including SiO_2 aerogels (Ref. [12]), PU aerogels (Refs. [18,19]), polymer/SiO_2 aerogels (Refs. [13–17]), nanocellulose aerogels (Ref. [21]), cellulose aerogels (Ref. [22]), RF aerogel (Refs. [27–29]), polymeric woods (Ref. [31]), polyimide aerogels (Refs. [33,38]).

Adding SiO_2 nanoparticles into PI aerogels can further decrease the thermal conductivity. The PI/SiO_2-2 composite aerogel with a density of 0.07 mg cm^{-3} can achieve a lower thermal conductivity of 21.8 mW m^{-1} K^{-1}, in contrast to 26.0 mW m^{-1} K^{-1} for air, 30.8 mW m^{-1} K^{-1} for aromatic polyimide aerogels [34], 26 mW m^{-1} K^{-1} for polyimide fiber sponges [5], 31.8 mW m^{-1} K^{-1} for polyimide aerogels [47] under ambient conditions. This super-insulation property of PI/SiO_2-2 composite aerogel can be explained by the following factors. The thermal conductivity can be divided into several contributions related to conduction (λ_{cond}), convection (λ_{conv}), and radiation (λ_{rad}). Due to the low application temperature, radiative heat transfer is neglected in the following analysis. A simple theoretical model can be used to estimate the effective thermal conductivity of the PI-based aerogels:

$$\lambda = \frac{\lambda_s \lambda_g}{(1-\varphi)\lambda_g + \varphi\lambda_s} \quad (1)$$

where φ is the porosity of aerogel, λ_g is the thermal conductivity of gas, and λ_s is the solid thermal conductivity, respectively.

The thermal conductivity of gas is strongly dependent on the pore size and can be estimated according to the following equation:

$$\lambda_g = \frac{\lambda_{g0}}{1 + 2\alpha l/D} \quad (2)$$

where λ_{g0} = 26.0 mW m^{-1} K^{-1} is the thermal conductivity of gas in the free space, $\alpha \approx 2$ for air, l is the mean free path of gas (~70 nm at ambient condition) and D is the mean pore size.

PI/SiO_2-2 composite aerogel exhibits a high porosity up to 96%, which contributes to low thermal conductivity according to Eq. (1). Furthermore, PI/SiO_2-2 composite aerogel has a smaller pore size as compared with the other samples (Fig. 2), which favors the reduction of gas conduction (λ_g) according to Eq. (2). Furthermore, smaller pore size contributes to numerous solid-air interfaces, which leads to tortuous photon conduction and multiple scattering at interfaces, resulting in enhanced thermal insulation behavior. In addition, the incorporation of nanosized components (SiO_2) leads to interfacial thermal resistance, the so-called Kapitza resistance, resulting reduction of the solid conduction of the walls [2]. Therefore, benefiting from its high porosity and tortuous porous channels, reduced pore size as well as nanostructure, the PI/SiO_2 composite aerogel exhibits excellent thermal insulation behavior at ambient temperature, much better than that (25 mW m^{-1} K^{-1}) of the most common super-insulating criterion.

Owing to the excellent thermal stability of PI/SiO_2 composite aerogel, which exhibits a high decomposition temperature up to 560 °C (Fig. S8), it shows good thermal insulation performance even at high temperatures. The thermal conductivity of PI/SiO_2-2 composite aerogel only shows a slight increase as the temperature goes up, with a low thermal conductivity of 33.2 mW m^{-1} K^{-1} at 300 °C (Fig. 4b). In contrast, pure PI aerogel shows a much faster increase of thermal conductivity, with a thermal conductivity more than 100 mW m^{-1} K^{-1} at 300 °C. This high-temperature insulation performance of PI/SiO_2 composite aerogel offers great superiority over current insulating materials. Fig. 4c compares PI/SiO_2-2 composite aerogel with many frequently used organic aerogel materials in thermal conductivity versus maximum working temperature. As shown in Fig. 4c, most polymeric insulation materials such as PU, cellulose or resorcinol-formaldehyde (RF) aerogels are easily collapsed at temperatures above 400 °C, which limit their further application under high temperatures. In contrast, our

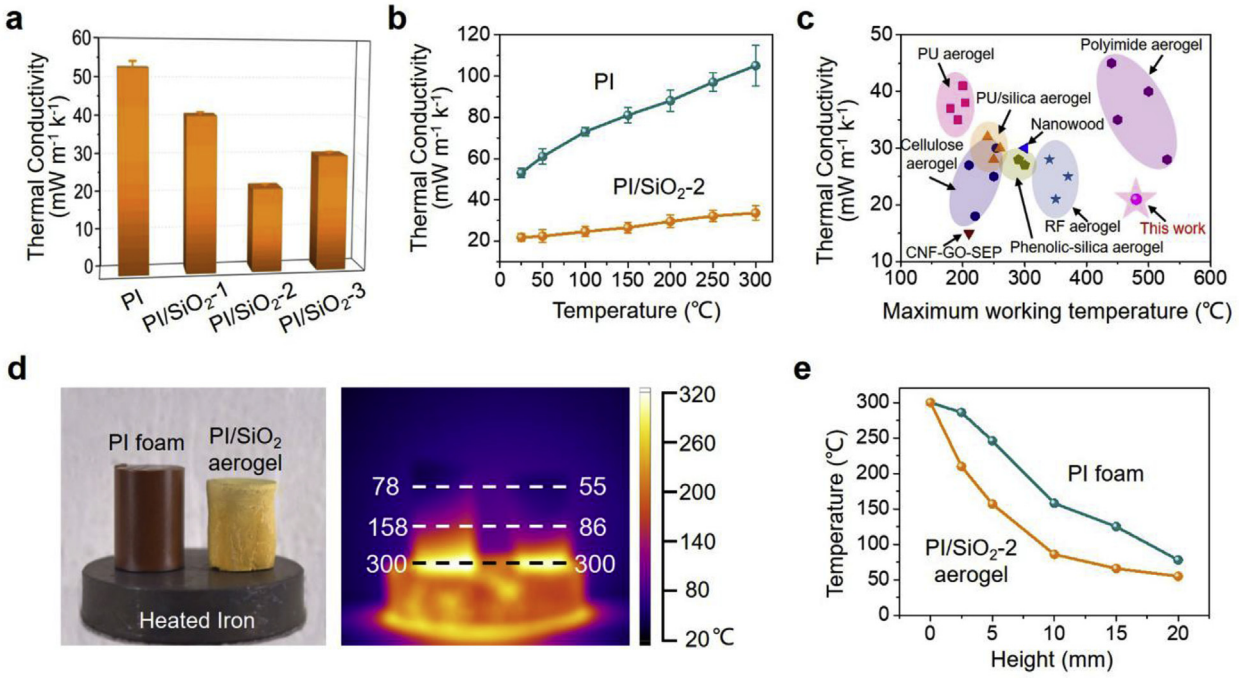

Fig. 4. Thermal insulation performance of PI/SiO_2 aerogels. (a) Thermal conductivity of PI, PI/SiO_2-1, PI/SiO_2-2, and PI/SiO_2-3 aerogels under ambient temperature. (b) Thermal conductivity of PI and PI/SiO_2-2 aerogels under different temperatures from 25 to 300 °C. (c) Thermal conductivity versus maximum working temperature for aerogel-like materials, including PU aerogels (Refs. [18–20]), cellulose aerogels (Refs. [21,22]), PU/silica aerogels (Ref. [17]), cellulose nanofibers-graphene oxide-sepiolite nanorods (CNF-GO-SEP) (Ref. [2]), nanowood (Ref. [1]), phenolic-silica aerogels (Ref. [27]), RF aerogels (Refs. [29,30]), polyimide aerogels (Refs. [34,38]). (d) Optical and infrared images of commercial PI foam and PI/SiO_2-2 aerogel on a 300 °C heating stage for 10 min. (e) Temperature versus height of PI foam and PI/SiO_2-2 aerogel obtained from infrared images.

PI/SiO_2 composite aerogel can be stable up to 480 °C while still remaining a low thermal conductivity. It is worth to mention that although the maximum working temperature of this organic PI based aerogel is lower than traditional ceramic aerogels, such as SiO_2, Al_2O_3, and ZrO_2, which exhibit excellent heat resistance up to 1200 °C, our PI/SiO_2 composite aerogel shows much better mechanical properties (Fig. 3e) that is very important for practical applications. As a proof of concept for thermal insulation applications, the PI/SiO_2 composite aerogel is placed on a hot stage comparing to commercial PI foam. After stabilization for 10 min, the temperature distribution of the PI/SiO_2 composite aerogel upon heating is monitored by infrared camera. As indicated in Fig. 4d, the top of PI/SiO_2 composite aerogel (20 mm thick) maintains a relatively low temperature of about 55 °C after being placed on a 300 °C heating stage, much lower than that (78 °C) of PI foam. Moreover, with the height increase, the PI/SiO_2 aerogel exhibits a much quicker temperature decrease inside as compared to PI foam (Fig. 4e), indicating its excellent thermal insulation ability even at a small thickness. Therefore, their outstanding thermal insulation in a wide temperature range and the excellent mechanical performance place PI/SiO_2 composite aerogels among the state-of-the-art thermal insulators.

4. Conclusions

In summary, thermal insulating PI/SiO_2 composite aerogels have been synthesized by freeze-drying method followed by thermal imidization. The amino functionalized SiO_2 nanoparticles behaving like crosslinkers could inhibit shrinkage (< 20%) and maintain high porosity (> 95%) of aerogels, resulting in PI/SiO_2 composite aerogels with good structure stability and a uniform porous structure. The highly porous structure and nanosized components (SiO_2 nanoparticles) benefit the reduction of thermal conductivity through inhibiting gas conduction and imparting interfacial thermal resistance, respectively. Consequently, the PI/SiO_2 aerogel with a low density exhibits good mechanical properties with specific compression modulus as high as 334 kN m kg^{-1}, which is among the highest level in aerogel materials. More importantly, the PI/SiO_2 composite aerogels show super-insulation properties in a wide temperature range with a low thermal conductivity of 21.8 and 33.2 mW m^{-1} K^{-1} at room temperature and 300 °C, respectively. The PI/SiO_2 composite aerogel with excellent mechanical and super-insulation properties may find broad applications in many civil and military fields.

Acknowledgments

The authors are grateful for the financial support from the National Natural Science Foundation of China (21674019, 21704014, 51433001), the Fundamental Research Funds for the Central Universities (2232017D-06), Shanghai Municipal Education Commission (17CG33), Shanghai Sailing Program (17YF1400200), Ministry of Education of the People's Republic of China (6141A0202202), Program of Shanghai Academic Research Leader (17XD1400100), and Science and Technology Commission of Shanghai Municipality (16520722100).

Appendix A. Supplementary data

Supplementary data to this article can be found online at https://doi.org/10.1016/j.compscitech.2019.01.025.

References

[1] T. Li, J. Song, X. Zhao, Z. Yang, G. Pastel, S. Xu, C. Jia, J. Dai, C. Chen, A. Gong, F. Jiang, Y. Yao, T. Fan, B. Yang, L.W. Gberg, R. Yang, L.B. Hu, Anisotropic, lightweight, strong, and super thermally insulating nanowood with naturally aligned nanocellulose, Sci. Adv. 4 (2018) 3724.
[2] B. Wicklein, A. Kocjan, G. Salazar-Alvarez, F. Carosio, G. Camino, M. Antonietti, L. Bergström, Thermally insulating and fire-retardant lightweight anisotropic foams based on nanocellulose and graphene oxide, Nat. Nanotechnol. 10 (2014) 277–283.
[3] E. Cuce, P.M. Cuce, C.J. Wood, S.B. Riffat, Toward aerogel based thermal

superinsulation in buildings: a comprehensive review, Renew. Sustain. Energy Rev. 34 (2014) 273–299.
[4] Y. Si, J. Yu, X. Tang, J. Ge, B. Ding, Ultralight nanofibre-assembled cellular aerogels with superelasticity and multifunctionality, Nat. Commun. 5 (2014).
[5] S.H. Jiang, B. Uch, S. Agarwal, A. Greiner, Ultralight, thermally insulating, compressible polyimide fiber assembled sponges, ACS Appl. Mater. Interfaces 9 (2017) 32308–32315.
[6] Y. Cui, H. Gong, Y. Wang, D. Li, H. Bai, A thermally insulating textile inspired by polar bear hair, Adv. Mater. 30 (2018) 1706807.
[7] L. Zhang, H. Deng, Q. Fu, Recent progress on thermal conductive and electrical insulating polymer composites, Compos. Commun. 8 (2018) 74–82.
[8] F. Bai, J. Wu, G. Gong, L. Guo, A flexible, sandwiched high-performance super-insulation fabric, J. Mater. Chem. A 3 (2015) 13198–13202.
[9] L.Z. Zuo, Y.F. Zhang, L.S. Zhang, Y.E. Miao, W. Fan, T.X. Liu, Polymer/Carbon-Based hybrid aerogels: preparation, properties and applications, Materials 8 (2015) 6806–6848.
[10] Z.L. Yu, G. Li, N. Fechler, N. Yang, Z.Y. Ma, X. Wang, M. Antonietti, S.H. Yu, Polymerization under hypersaline conditions: a robust route to phenolic Polymer-Derived carbon aerogels, Angew. Chem. Int. Ed. 55 (2016) 14623–14627.
[11] Y. Si, X.Q. Wang, L.Y. Dou, J.Y. Yu, B. Ding, Ultralight and fire-resistant ceramic nanofibrous aerogels with temperature-invariant superelasticity, Sci. Adv. 4 (2018) 8925.
[12] J.C.H. Wong, H. Kaymak, S. Brunner, M.M. Koebel, Mechanical properties of monolithic silica aerogels made from polyethoxydisiloxanes, Microporous Mesoporous Mater. 183 (2014) 23–29.
[13] S. Zhao, Z. Zhang, G. Sèbe, R. Wu, R.V. Rivera Virtudazo, P. Tingaut, M.M. Koebel, Multiscale assembly of superinsulating silica aerogels within silylated nanocellulosic scaffolds: improved mechanical properties promoted by nanoscale chemical compatibilization, Adv. Funct. Mater. 25 (2015) 2326–2334.
[14] S. Zhao, W.J. Malfait, A. Demilecamps, Y. Zhang, S. Brunner, L. Huber, P. Tingaut, A. Rigacci, T. Budtova, M.M. Koebel, Strong, thermally superinsulating Biopolymer-Silica aerogel hybrids by cogelation of silicic acid with pectin, Angew. Chem. Int. Ed. 54 (2015) 14282–14286.
[15] A. Katti, N. Shimpi, S. Roy, H. Lu, E.F. Fabrizio, A. Dass, L.A. Capadona, N. Leventis, Chemical, physical, and mechanical characterization of isocyanate cross-linked Amine-Modified silica aerogels, Chem. Mater. 18 (2006) 285–296.
[16] M.A.B. Meador, L.A. Capadona, L. McCorkle, D.S. Papadopoulos, N. Leventis, Structure-Property relationships in porous 3D nanostructures as a function of preparation conditions: isocyanate Cross-Linked silica aerogels, Chem. Mater. 19 (2007) 2247–2260.
[17] G. Churu, B. Zupančič, D. Mohite, C. Wisner, H. Luo, I. Emri, C. Sotiriou-Leventis, N. Leventis, H. Lu, Synthesis and mechanical characterization of mechanically strong, polyurea-crosslinked, ordered mesoporous silica aerogels, J. Sol Gel Sci. Technol. 75 (2015) 98–123.
[18] N. Diascorn, S. Calas, H. Sallée, P. Achard, A. Rigacci, Polyurethane aerogels synthesis for thermal insulation – textural, thermal and mechanical properties, J. Supercrit. Fluids 106 (2015) 76–84.
[19] C. Chidambareswarapattar, P.M. McCarver, H. Luo, H. Lu, C. Sotiriou-Leventis, N. Leventis, Fractal multiscale nanoporous polyurethanes: flexible to extremely rigid aerogels from multifunctional small molecules, Chem. Mater. 25 (2013) 3205–3224.
[20] H. Zhang, W.Z. Fang, Y.M. Li, W.Q. Tao, Experimental study of the thermal conductivity of polyurethane foams, Appl. Therm. Eng. 115 (2017) 528–538.
[21] Y. Kobayashi, T. Saito, A. Isogai, Aerogels with 3D ordered nanofiber skeletons of Liquid-Crystalline nanocellulose derivatives as tough and transparent insulators, Angew. Chem. Int. Ed. 53 (2014) 10394–10397.
[22] Q.Y. Mi, S.R. Ma, J. Yu, J.S. He, J. Zhang, Flexible and transparent cellulose aerogels with uniform nanoporous structure by a controlled regeneration process, ACS Sustain. Chem. Eng. 4 (2016) 656–660.
[23] T. Nissilä, S.S. Karhula, S. Saarakkala, K. Oksman, Cellulose nanofiber aerogels impregnated with bio-based epoxy using vacuum infusion: structure, orientation and mechanical properties, Compos. Sci. Technol. 155 (2018) 64–71.
[24] C. Ma, B. Du, E. Wang, Self-Crosslink method for a straightforward synthesis of Poly (Vinyl Alcohol)-Based aerogel assisted by carbon nanotube, Adv. Funct. Mater. 27 (2017) 1604423.
[25] W. Guo, J. Liu, P. Zhang, L. Song, X. Wang, Y. Hu, Multi-functional hydroxyapatite/polyvinyl alcohol composite aerogels with self-cleaning, superior fire resistance and low thermal conductivity, Compos. Sci. Technol. 158 (2018) 128–136.
[26] X. Wang, L.L. Lu, Z.L. Yu, X.W. Xu, Y.R. Zheng, S.H. Yu, Scalable template synthesis of Resorcinol-Formaldehyde/Graphene oxide composite aerogels with tunable densities and mechanical properties, Angew. Chem. Int. Ed. 54 (2015) 2397–2401.
[27] Z.L. Yu, N. Yang, V. Apostolopoulou-Kalkavoura, B. Qin, Z. Ma, W. Xing, C. Qiao, L. Bergström, M. Antonietti, S.H. Yu, Fire-Retardant and thermally insulating Phenolic-Silica aerogels, Angew. Chem. Int. Ed. 57 (2018) 4538–4542.
[28] J. Yang, S. Li, L. Yan, J. Liu, F. Wang, Compressive behaviors and morphological changes of resorcinol-formaldehyde aerogel at high strain rates, Microporous Mesoporous Mater. 133 (2010) 134–140.
[29] S. Berthon-Fabry, C. Hildenbrand, P. Ilbizian, E. Jones, S. Tavera, Evaluation of lightweight and flexible insulating aerogel blankets based on Resorcinol-Formaldehyde-Silica for space applications, Eur. Polym. J. 93 (2017) 403–416.
[30] S. Berthon-Fabry, C. Hildenbrand, P. Ilbizian, Lightweight superinsulating Resorcinol-Formaldehyde-APTES benzoxazine aerogel blankets for space applications, Eur. Polym. J. 78 (2016) 25–37.
[31] Z.L. Yu, N. Yang, L. Zhou, Z. Ma, Y. Zhu, Y. Lu, B. Qin, W. Xing, T. Ma, S. Li, H. Gao, H.A. Wu, S.H. Yu, Bioinspired polymeric woods, Sci. Adv. 4 (2018) 7223.
[32] X. Li, J. Wang, Y. Zhao, X.T. Zhang, Template-Free Self-Assembly of Fluorine-Free hydrophobic polyimide aerogels with lotus or petal effect, ACS Appl. Mater. Interfaces 10 (2018) 16901–16910.
[33] M.A.B. Meador, C.R. Alemán, K. Hanson, N. Ramirez, S.L. Vivod, N. Wilmoth, L. McCorkle, Polyimide aerogels with amide Cross-Links: a low cost alternative for mechanically strong polymer aerogels, ACS Appl. Mater. Interfaces 7 (2015) 1240–1249.
[34] J.Z. Feng, X. Wang, Y.G. Jiang, D.X. Du, J. Feng, Study on thermal conductivities of aromatic polyimide aerogels, ACS Appl. Mater. Interfaces 8 (2016) 12992–12996.
[35] L.L. Xu, L.H. Xiao, P. Jia, K. Goossens, P. Liu, H. Li, C.G. Cheng, Y. Huang, C.W. Bielawski, J.X. Geng, Lightweight and ultrastrong polymer foams with unusually superior flame retardancy, ACS Appl. Mater. Interfaces 9 (2017) 26392–26399.
[36] J.G. Kim, J. Lee, J. Lee, S.I. Jo, J.Y. Chang, A hierarchically porous polyimide composite prepared by one-step condensation reaction inside a sponge for heterogeneous catalysis, Macromol. Res. 25 (2017) 629–634.
[37] T. Huh, S.Y. Lee, S.K. Park, J. Chang, Y. Lee, Y. Kwark, Homogeneous Polyimide/Silica nanohybrid films adapting simple polymer blending process: polymeric silsesquiazane precursor to inorganic silica, Macromol. Res. 26 (2018) 187–193.
[38] J.C. Williams, B.N. Nguyen, L. McCorkle, D. Scheiman, J.S. Griffin, S.A. Steiner, M.A.B. Meador, Highly porous, Rigid-Rod polyamide aerogels with superior mechanical properties and unusually high thermal conductivity, ACS Appl. Mater. Interfaces 9 (2017) 1801–1809.
[39] W. Fan, L.Z. Zuo, Y.F. Zhang, Y. Chen, T.X. Liu, Mechanically strong polyimide/carbon nanotube composite aerogels with controllable porous structure, Compos. Sci. Technol. 156 (2018) 186–191.
[40] L.Z. Zuo, W. Fan, Y.F. Zhang, L.S. Zhang, W. Gao, Y.P. Huang, T.X. Liu, Graphene/montmorillonite hybrid synergistically reinforced polyimide composite aerogels with enhanced flame-retardant performance, Compos. Sci. Technol. 139 (2017) 57–63.
[41] K. Haraguchi, H. Li, Mechanical properties and structure of Polymer-Clay nanocomposite gels with high clay content, Macromolecules 39 (2006) 1898–1905.
[42] J. Oh, J. Kim, H. Lee, Y. Kang, I. Oh, Directionally antagonistic graphene Oxide-Polyurethane hybrid aerogel as a sound absorber, ACS Appl. Mater. Interfaces 10 (2018) 22650–22660.
[43] M. Kim, K. Eo, H.J. Lim, Y.K. Kwon, Low shrinkage, mechanically strong polyimide hybrid aerogels containing hollow mesoporous silica nanospheres, Compos. Sci. Technol. 165 (2018) 355–361.
[44] S. Wu, A. Du, Y. Xiang, M. Liu, T. Li, J. Shen, Z. Zhang, C. Li, B. Zhou, Silica-aerogel-powders "jammed" polyimide aerogels with excellent hydrophobicity and conversion to ultra-light polyimide aerogel, RSC Adv. 6 (2016) 58268–58278.
[45] S.Y. Kim, Y.J. Noh, J. Lim, N. You, Silica aerogel/polyimide composites with preserved aerogel pores using multi-step curing, Macromol. Res. 22 (2014) 108–111.
[46] P. Yan, B. Zhou, A. Du, Synthesis of polyimide cross-linked silica aerogels with good acoustic performance, RSC Adv. 4 (2014) 58252–58259.
[47] Z. Qian, Z. Wang, Y. Chen, S. Tong, M. Ge, N. Zhao, J. Xu, Superelastic and ultralight polyimide aerogels as thermal insulators and particulate air filters, J. Mater. Chem. A 6 (2018) 828–832.